sustainability

MDPI

Article

Synthesis and Basic Properties of $Y_{1-x}Yb_xVO_4$ Obtained by High-Energy Ball Milling and High-Temperature Treatment

Mateusz Piz [1,*], Elżbieta Filipek [1], Daniel Klukowski [2] and Paweł Kochmański [3]

[1] Department of Inorganic and Analytical Chemistry, Faculty of Chemical Technology and Engineering, West Pomeranian University of Technology in Szczecin, al. Piastów 42, 71-065 Szczecin, Poland
[2] Department of Geoinformatics, Faculty of Navigation, Maritime University of Szczecin, Wały Chrobrego 1-2, 70-500 Szczecin, Poland
[3] Faculty of Mechanical Engineering and Mechatronics, West Pomeranian University of Technology in Szczecin, al. Piastów 19, 70-310 Szczecin, Poland
* Correspondence: mpiz@zut.edu.pl

Abstract: The main objective of this work was to experimentally confirm that a continuous, substitutional solid solution of a general formula $Y_{1-x}Yb_xVO_4$ is formed in the pseudo-binary system YVO_4–$YbVO_4$, and to investigate its basic unknown properties as a function of composition for $0.00 < x < 1.00$. To date, such a solid solution has been obtained and characterized to a limited extent, but only for a few selected compositions. This solution was obtained by a high temperature and, for the first time, using mechanochemical methods. For the solution obtained by the high-energy ball-milling method, unknown physicochemical properties were established over its entire range of homogeneity. The solution was synthesized from mixtures of yttrium orthovanadate (V) with ytterbium (III) orthovanadate (V) of different compositions and investigated by XRD, IR, SEM, and UV-Vis(DRS) methods. It was found that $Y_{1-x}Yb_xVO_4$ crystallizes in a tetragonal system. The results confirmed that the solid solution $Y_{1-x}Yb_xVO_4$ has a structure of YVO_4 and $YbVO_4$, and its structure is composed of YbO_6 and YO_6 octahedrons and VO_4 tetrahedrons. Moreover, if the parameter (x) in the solid solution $Y_{1-x}Yb_xVO_4$ increases, its crystalline lattice contracts and the value of the energy gap decreases. This solid solution is stable in the air atmosphere at least up to ~1500 °C. The estimated band gap for this solid solution indicates that it belongs to the semiconductors.

Keywords: solid solution $Y_{1-x}Yb_xVO_4$; mechanochemical synthesis; XRD; UV-VIS/DRS; semiconductors

Citation: Piz, M.; Filipek, E.; Klukowski, D.; Kochmański, P. Synthesis and Basic Properties of $Y_{1-x}Yb_xVO_4$ Obtained by High-Energy Ball Milling and High-Temperature Treatment. *Sustainability* **2023**, *15*, 14606. https://doi.org/10.3390/su151914606

Academic Editor: Manal Rawashdeh-Omary

Received: 28 July 2023
Revised: 19 September 2023
Accepted: 28 September 2023
Published: 9 October 2023

1. Introduction

In recent decades, comprehensive and intensive research has been conducted, encompassing both theoretical and experimental approaches. The findings from these studies have led to the development of technologies producing new functional materials with the expected catalytic, magnetic, mechanical, electrical, or optical properties. Such new materials, undoubtedly competing with those used so far, should be characterized by improved desired properties, simultaneously with low-cost, waste-free, pro-ecological, and easily available manufacturing. Therefore, the dopant modification of the already existing material is a common method used for a new material development.

The mechanochemical method meets most of the requirements of "green chemistry", as it does not generate harmful waste for disposal and is environmentally friendly. Its main advantage is simplicity, since the method is based on milling various types of substances in a high-energy mill. The mechanical energy generated during grinding is delivered to the substrates and accumulates in them in the form of all kinds of lattice stresses and defects, which can increase their reactivity. The process of high-energy grinding can lead to very fine grinding of the product, often down to nanoparticles. High-energy ball milling

has been successfully used to synthesize many new functional materials, such as alloys, intermetallic compounds, polymers, and ceramic materials [1–4].

Among the diverse objects whose research is directed at the search for new functional materials, a significant group is bicomponent, ternary, and even quaternary systems of metal oxides. The choice of a given system for research is very often determined by the application-requiring modification of the properties of its components, i.e., oxides, as well as known compounds formed in binary systems that are lateral constraints of multicomponent systems. An example of a binary system constituting one cross-section of a ternary system of V_2O_5–Yb_2O_3–Y_2O_3 oxides is the YVO_4–$YbVO_4$ system [5–30]. Yttrium orthovanadate(V) and ytterbium are well characterized in the literature [27–46]. Methods for their syntheses are known, ranging from the solid-state reaction method to hydrothermal, Pechini, or co-precipitation [5,6,9,15–17,27,34,41]. It is also known that YVO_4 and $YbVO_4$ crystallize in a tetragonal system [7,11,30–32,35]. Depending on studies, the congruent melting temperature of YVO_4 varies from 1780 to 1810 °C, while $YbVO_4$ melts at ~1820 °C [18,19].

Literature data on yttrium orthovanadate(V) indicate that this compound doped with Ce^{3+}, Eu^{3+}, Dy^{3+}, Sm^{3+}, or Er^{3+} ion results in materials able to be applied in high-resolution devices, such as cathode ray tubes (CRT), flat panel displays, and field emission displays (FED) [20,36,37,39,42–46]. Data on the properties of YVO_4 also point out that the compound is a useful matrix for the listed rare earth ions, making it possible to produce phosphors that emit light of different colors [20,21,33,42]. Yttrium orthovanadate(V) activated with Eu^{3+} ions is an important red phosphor used in color television, cathode ray tubes, and high-pressure mercury lamps. On the other hand, YVO_4 activated with Dy^{3+} ions is a potential component of white phosphors and Nd^{3+} ions of blue ones [20,33,37].

Ytterbium orthovanadate(V), like yttrium orthovanadate(V), is an important optical material. Doping YVO_4 with ytterbium ions and using it as a host material is a promising solution in the prospect of developing a low-threshold and high-performance solid-state erbium laser [12,20,38,40,41]. It is also possible to dope orthovanadium(V) ytterbium with other rare earth ions, such as neodymium, to produce lasers with a wavelength of 1.35 µm. $YbVO_4$ crystals doped with neodymium can produce red, green, or blue light with high efficiency and beam quality [13,20]. The phases obtained in the work are most often with general formulas YVO_4:Yb^{3+} and Yb:YVO_4. The methods for obtaining such phases do not differ significantly from those for the synthesis of pure yttrium and ytterbium orthovanadates(V) [5,6,16,17,28,38]. The doping of YVO_4 with Yb^{3+} ions using ytterbium orthovanadate(V) is rare, and if so, it is in a limited range of $YbVO_4$ concentrations, namely in the range of 0.4 to 25% molar of orthovanadate(V) in a mixture with YVO_4 [22–25]. In summary, to our knowledge and based on the performed literature review, comprehensive studies of the reactivity of yttrium orthovanadate(V) with ytterbium orthovanadate(V) over the entire concentration range of the components of the system comprising these compounds—i.e., in the YVO_4–$YbVO_4$ system—have not yet been carried out.

The published works [22–25] show that only a few samples from the mentioned system have been tested so far, including those containing no more than 25.00 mol% of Yb^{3+} ions in the YVO_4 crystal lattice, corresponding to the $Y_{1-x}Yb_xVO_4$ solid solution for $0.004 < x < 0.25$. Importantly, the study, mostly focused on monocrystalline samples, primarily examined their optical properties.

Taking into account the fact that the components of the YVO_4–$YbVO_4$ system are isostructural, and that the Y^{3+} and Yb^{3+} ions present in their structures have similar values of ionic radii (Yb^{3+}—86.8 pm, Y^{3+}—90.0 pm), the primary objective of our work was to experimentally demonstrate that a continuous substitutional solid solution with the general formula $Y_{1-x}Yb_xVO_4$ is formed in the YVO_4–$YbVO_4$ system. As the sustainability of solid solution $Y_{1-x}Yb_xVO_4$ is not known, the DTA-TGA measurements in the air atmosphere and in the temperature range 25–1500 °C were performed. In this range, no thermal effects were observed on DTA and TG curves. The results prove that the obtained phase is stable in an air atmosphere at least up to ~1500 °C. Considering the fact that for the first

time the mechanochemical method was used to obtain the solid solution, an additional objective was to study the effect of the degree of incorporation of Yb^{3+} (x) ions into the YVO_4 crystal lattice on the physicochemical properties of the $Y_{1-x}Yb_xVO_4$ solution, i.e., lattice parameters, density, particle size distribution, or energy gap value, etc. The results presented in this work have significantly advanced the knowledge of the solid solution formed in the YVO_4–$YbVO_4$ system. It was shown that the $Y_{1-x}Yb_xVO_4$ solid solution forms over the entire concentration range of the components of the studied system, i.e., for $0.00 < x < 1.00$, and not only for $0.004 < x < 0.25$. For the first time, such a nanometric solution was obtained mechanochemically. The unknown properties of the solution obtained both by high-temperature and mechanochemical methods were examined as a function of its composition.

2. Materials and Methods

The reagents used in our experiments are YVO_4 and $YbVO_4$, which were synthesized from the oxides Y_2O_3, a.p. (Alfa Aesar, Memphis, TN, USA), Yb_2O_3, a.p. (Alfa Aesar, Memphis, TN, USA), and V_2O_5, a.p. (POCh, Poland) by the mechanochemical and high-temperature methods described in refs. [1,22–24,30–32]. For the experiments, 10 samples were prepared from separately obtained YVO_4 and $YbVO_4$ (Table 1) by using two different methods:

Table 1. Composition of initial mixtures and results of phase analysis of samples after the last stage of their ball milling and high-temperature treatment.

No.	% mol		x in $Y_{1-x}Yb_xVO_4$	Phase Composition of Samples after Synthesis by High-Energy Ball Milling and High-Temperature Treatment
	YVO_4	$YbVO_4$		
1	90.00	10.00	0.10	$Y_{0.90}Yb_{0.10}VO_4$
2	75.00	25.00	0.25	$Y_{0.75}Yb_{0.25}VO_4$
3	50.00	50.00	0.50	$Y_{0.50}Yb_{0.50}VO_4$
4	25.00	75.00	0.75	$Y_{0.25}Yb_{0.75}VO_4$
5	10.00	90.00	0.90	$Y_{0.10}Yb_{0.90}VO_4$

(a) Mechanochemical synthesis (MECh) using laboratory planetary ball mill *Pulverisette-6* (Fritsch GmbH, Idar-Oberstein, Germany) with vessel and balls of zirconia, rpm = 500, BPR = 1:20, time = 3.0 and once again 3.0 hrs under air atmosphere.

(b) High-temperature treatment (HTH) in a horizontal tube furnace PRC 50/170/M (Czylok, Jastrzębie-Zdrój, Poland) equipped with a stationary optical pyrometer MARATHON MM (Raytek, Wilmington, North Carolina, USA). Reagents weighed in suitable proportions were homogenized and calcined in the air atmosphere in the temperature range 1000–1500 °C. After each heating stage, the samples were gradually cooled in the furnace to room temperature by the method described, e.g., in [47–50].

The powder diffraction patterns of the samples obtained were recorded on a diffractometer EMPYREAN II (PANalytical, Almelo, The Netherlands) using CuK_α with a graphite monochromator (2θ range 7–45°); time of counting 71.40 s, step 0.013.

The phases were identified on the basis of XRD characteristics contained in the PDF cards (Powder Diffraction File4+).

The parameters of selected unit cell solid solutions were refined using the REFINEMENT program of the DHN/PDS package.

Selected samples were examined using the following methods:

– SEM using an FE-SEM Hitachi SU–70 microscope. Analyses were performed at an accelerating voltage of 5 and 15 kV and secondary electron images were acquired. (Thermo Fisher Scientific); the blowup of the SEM images was 20.000 and 100.000.

- IR—the measurements were made within the wavenumber range of 1200–400 cm^{-1}, using a spectrophotometer Nicolet iS5 (ThermoFisher, Memphis, TN, USA). The technique of pressing pellets with KBr at the mass ratio of 1:300 was applied.
- LDS using Mastersizer 3000 (Malvern Panalytical, Malvern, UK), He-Ne laser (λ = 632.8 nm), LED (λ = 470.0 nm),
- UV-Vis-DR spectra were measured using a UV-Vis spectrometer V-670 (JASCO, Japan) equipped with a reflecting attachment for the solid-state investigation (integrating sphere attachment with horizontal sample platform PIV-756/(PIN-757). The spectra were recorded in the wavelength region of 200–750 nm at room temperature.

The densities of solid solutions were determined in argon (5N purity) with the help of an Ultrapyc 1200e ultrapycnometer (Quantachrome Instruments, Boynton Beach, FL, USA).

The crystallite sizes of the solid solution were determined by using the Scherrer method according to the equation: $L = K\lambda/\beta \cdot Cos\theta$. The size of the nanocrystallites (L) was calculated using XRD radiation of the wavelength of λ (nm) from measuring the full width at half maximum of the peaks (β) in radians located at any 2θ in the pattern.

3. Results and Discussion

3.1. Mechanochemical Synthesis

The study of the YVO_4–$YbVO_4$ system began with the preparation of five mixtures of YVO_4 with $YbVO_4$ with the compositions shown in Table 1. The compositions of these samples were chosen to represent different ranges of concentrations of the components of the system under study.

Mixtures of isostructural vanadates, i.e., yttrium and ytterbium, were subjected to mechanochemical synthesis carried out in a high-energy planetary ball mill under an air atmosphere in two 3 h stages. An X-ray phase analysis of all samples proved a change in the initial composition after the first milling stage. The individual diffraction lines recorded on the diffractograms of these samples, corresponded to the interplane distances d_{hkl}, whose values ranged from those identifying YVO_4 (PDF-card number: 04-007-6542), to those corresponding to $YbVO_4$ (PDF-cards number: 04-019-7298 and 04-008-3642). An analysis of the diffractograms of these samples therefore indicated that they were single phase and contained only a substitutional solid solution of YVO_4 or $YbVO_4$ structure. A subsequent 3 h milling step did not change the phase composition of all samples.

Based on the results obtained, it was found that a solid solution was obtained by the high-energy milling of mixtures of YVO_4 with $YbVO_4$ over the entire concentration range of the components of the system under study. Thus, it is a continuous substitution solid solution, the general formula of which can be written either as $Y_{1-x}Yb_xVO_{4(s.s.)}$ or as $Yb_{1-y}Y_yVO_{4(s.s.)}$. For the solution so obtained, in the further description of the results, it was assumed that the matrix of the continuous, substituted solid solution is the compound YVO_4.

Table 1 shows the compositions of the tested samples prepared from mixtures of YVO_4 with $YbVO_4$, before and after the last stage of their synthesis.

Following, the solution is formed by incorporating Yb^{3+} ions into the YVO_4 crystal lattice in place of Y^{3+} ions, according to the reaction:

$$(1 - x)\ YVO_{4\ (s)} + x\ YbVO_{4\ (s)} = Y_{1-x}Yb_xVO_{4(s.s.)} \quad (1)$$

Figure 1 presents fragments of the diffractograms of mechanochemically obtained compounds YVO_4 (Figure 1a) and $YbVO_4$ (Figure 1e), compared with fragments of the diffractograms of the $Y_{1-x}Yb_xVO_4$ solid solution obtained by the method for the first time for x = 0.10 (Figure 1b), x = 0.50 (Figure 1c), and x = 0.90 (Figure 1d).

The analysis of the diffractograms (XRD) of single-phase samples (Figure 1), i.e., those containing $Y_{1-x}Yb_xVO_{4(s.s.)}$ solid solution, showed that since the content of $YbVO_4$ increases in the initial mixtures of reactants, i.e., the value of x in the obtained solution, the XRD lines characterizing this phase are shifted toward higher angles 2Θ. This means

that they correspond to smaller values of interplane distances d_{hkl} relative to the X-ray characteristics of $YbVO_4$.

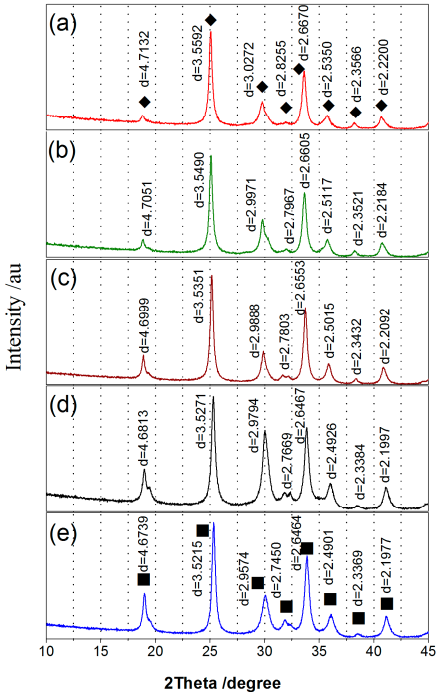

Figure 1. Fragments of diffractograms: (**a**) YVO_4 (◆ PDF-card no: 04-007-6542), (**b**) $Y_{0.90}Yb_{0.10}VO_4$, (**c**) $Y_{0.50}Yb_{0.50}VO_4$, (**d**) $Y_{0.10}Yb_{0.90}VO_4$, (**e**) $YbVO_4$ (■ PDF-cards no: 04-019-7298 and 04-008-3642).

This can be explained by the size of the radius of the Yb^{3+} ion in octahedral coordination, which equals 86.8 pm, which is smaller than the radius of the Y^{3+} ion, i.e., 90.0 pm. During the synthesis, a substitution of these ions takes place, leading to the contraction of the crystal lattice. These results are additional evidence for the formation of a substitutive continuous solid solution.

The extended diffraction lines in the diffractograms of the $Y_{1-x}Yb_xVO_4$ solid solution obtained for the first time by the mechanochemical method (Figure 2) indicate that the crystallites of the obtained phase are small in size. The crystallite sizes of mechanochemically synthesized $Y_{1-x}Yb_xVO_4$ determined using Scherrer's method are ~17 nm (x = 0.10), ~19 nm (x = 0.25), ~18 nm (x = 0.50), ~18 nm (x = 0.75), and ~15 nm (x = 0.90).

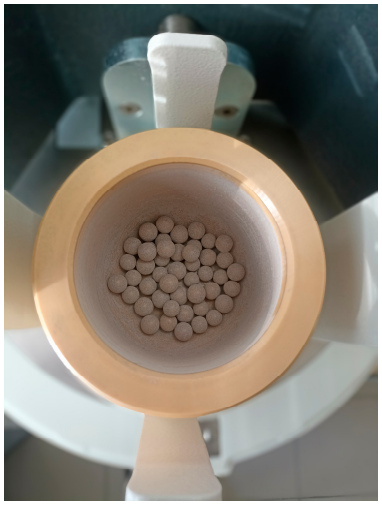

Figure 2. $Y_{1-x}Yb_xVO_4$ obtained in a ball mill.

The aim of the next stage of the study was to confirm that the $Y_{1-x}Yb_xVO_4$ solid solution synthesized for the first time by the mechanochemical method shows the crystalline structure of YVO_4 and $YbVO_4$, i.e., a tetragonal system. For this purpose, powder diffractograms of the obtained $Y_{1-x}Yb_xVO_4$ solution for x = 0.10, 0.25, 0.50, 0.75, and 0.90 were subjected to refinement using the REFINEMENT program. The results confirmed that the obtained solid solution crystallizes in a tetragonal system, and its lattice parameters were calculated as a function of the degree of incorporation of Yb^{3+} ions in place of Y^{3+} into the YVO_4 crystal lattice. Table 2 shows the calculated elementary cell parameters of their volumes and densities: X-ray and experimental for the synthesized solid solution.

Table 2. Unit cell parameters, volumes and densities of solid solution $Y_{1-x}Yb_xVO_4$ for x = 0.10, 0.25, 0.50, 0.75, and 0.90 obtained by mechanochemical method.

x in $Y_{1-x}Yb_xVO_4$	a, b [nm]	c [nm]	α, β, γ [°]	V [nm^3]	d_{xrd}/d_{exp} [g/cm^3]
0.10	0.70553	0.67501	90.00	0.3360	4.20/4.09 ± 0.05
0.25	0.70207	0.67435	90.00	0.3324	4.50/4.37 ± 0.05
0.50	0.70185	0.67130	90.00	0.3307	4.95/4.67 ± 0.05
0.75	0.69929	0.66908	90.00	0.3272	5.42/5.08 ± 0.05
0.90	0.69888	0.65875	90.00	0.3217	5.77/5.43 ± 0.05

As can be seen from the data shown in Table 2, with an increase in the x value in the $Y_{1-x}Yb_xVO_4$ formula, manifesting a higher incorporation degree of Yb^{3+} ions and lower of the Y^{3+}, the crystal lattice contracts and the volume of elementary cells decreases. Moreover, the density of the solid solution, determined using the gas ultrapycnometer, increases with an increase in the x value, which corresponds well with the calculated X-ray density. Close values obtained from two separate techniques substantiate the correctness of the selected solutions. Somewhat lower values of the experimental density are most likely a result of the measurement error originating, e.g., from the porosity and defects of the obtained material.

In a next step, both ytterbium orthovanadate(V) (Figure 3a) and yttrium (Figure 3b), as well as the $Y_{1-x}Yb_xVO_4$ solid solution for x = 0.50 (Figure 3c), were subjected to scanning electron microscopy (SEM) studies. Images of the obtained polycrystalline samples are shown in Figure 3.

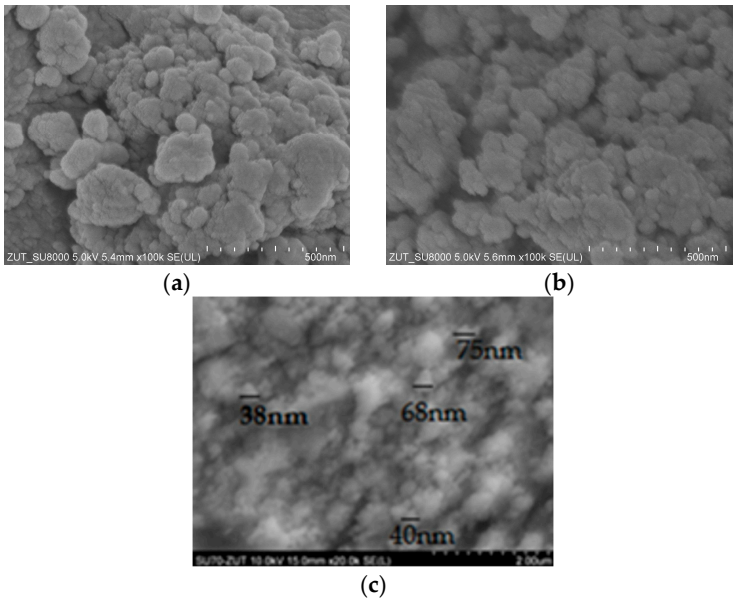

Figure 3. SEM images of (**a**) $YbVO_4$, (**b**) YVO_4, (**c**) $Y_{0.50}Yb_{0.50}VO_4$.

Visible in Figure 3, the crystallites of the $Y_{1-x}Yb_xVO_4$ solid solution for x = 0.50 are very similar to the crystallites of the substrates, i.e., $YbVO_4$ and YVO_4, in terms of their shape. In their appearance, they resemble irregular, very fine, "disordered" polyhedrons of varying sizes with the size of a significant part of them not exceeding 100 nm (Figure 3c).

The particle size distribution of the solid solution $Y_{1-x}Yb_xVO_4$, obtained by the mechanochemical method, was determined using the LDS method (Figure 4).

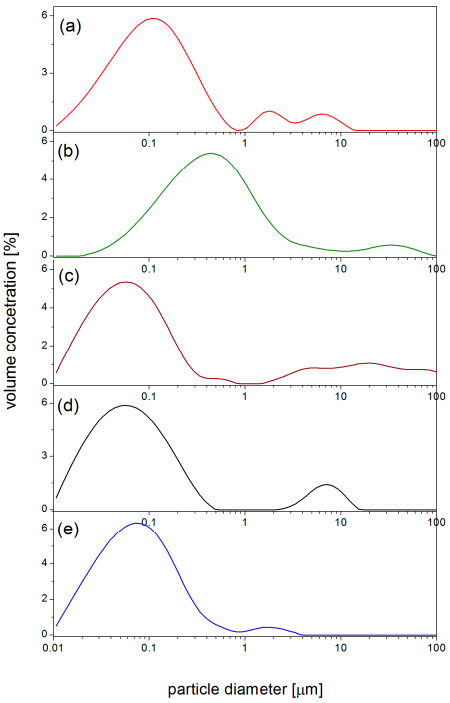

Figure 4. Particle size distribution curve of: (**a**) $Y_{0.90}Yb_{0.10}VO_4$, (**b**) $Y_{0.75}Yb_{0.25}VO_4$, (**c**) $Y_{0.50}Yb_{0.50}VO_4$, (**d**) $Y_{0.25}Yb_{0.75}VO_4$, (**e**) $Y_{0.10}Yb_{0.90}VO_4$.

Based on the LDS analysis (Figure 4, Table 3), the particle sizes of the $Y_{1-x}Yb_xVO_4$ solid solution were determined to be nanometer-sized, i.e., ~100 nm (including 10% of ~29 nm for x = 0.10), ~440 nm (including 10% of ~102 nm for x = 0.25), ~58 nm (including 10% of ~22 nm for x = 0.50), ~55 nm (including 10% of ~21 nm for x = 0.75), and ~75 nm (including 10% of ~21 nm for x = 0.90). According to the LDS curve, the $Y_{1-x}Yb_xVO_4$ solid solution was found to have bimodal distribution, that is, it does not have a homogeneous distribution. It is known that when a material is milled using high-energy ball milling technique, the milled material can be reduced to the nanosize and may have an inhomogeneous distribution [51,52].

Table 3. Particle sizes of solid solution.

Formula of Solid Solution	Particle Size [μm]		
	d_{90}	d_{50}	d_{10}
$Y_{0.90}Yb_{0.10}VO_4$	1.010	0.105	0.029
$Y_{0.75}Yb_{0.25}VO_4$	2.420	0.432	0.102
$Y_{0.50}Yb_{0.50}VO_4$	19.500	0.077	0.022
$Y_{0.25}Yb_{0.75}VO_4$	0.416	0.069	0.021
$Y_{0.10}Yb_{0.90}VO_4$	0.233	0.067	0.021

Next, it was determined which oxygen polyhedrons of yttrium and ytterbium comprise the structure of the mechanochemically obtained solution $Y_{1-x}Yb_xVO_4$. For this purpose, selected single-phase samples of the solution were studied by using infrared spectroscopy (IR). In addition to the IR spectra of the compounds YVO_4 (Figure 5a) and $YbVO_4$ (Figure 5e),

the IR spectra of the obtained solid solution $Y_{1-x}Yb_xVO_4$ for x = 0.10, 0.50, and 0.90 are also shown in the figure (Figure 5b–d, respectively).

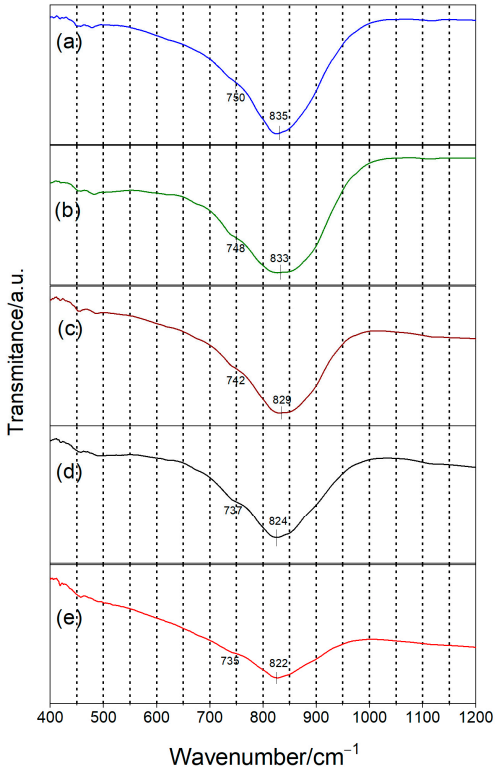

Figure 5. IR spectrum of: (**a**) YVO_4, (**b**) $Y_{0.90}Yb_{0.10}VO_4$, (**c**) $Y_{0.50}Yb_{0.50}VO_4$ (**d**) $Y_{0.10}Yb_{0.90}VO_4$, (**e**) $YbVO_4$.

In the IR spectra of the studied phases (in 400 to 1200 cm^{-1} wavenumber range), a broad absorption band (maxima of bands at 822–835 cm^{-1}) with an inflection on the side of lower wavenumbers (maxima of bands at 735–750 cm^{-1}) is present. Additionally, two very low intensity bands are also registered with maxima at around ~450 and 475 cm^{-1}, respectively. The broad band at ~830 cm^{-1}, according to literature data [14], is caused by stretching vibrations (ν) of V-O bonds in VO_4 tetrahedra. However, it cannot be ruled out that the recorded band with an inflection at ~750 cm^{-1} is also related to stretching vibrations of Y-O or Yb-O bonds in YO_6 or YbO_6 octahedra [53–55]. In contrast, the bands at ~450 and 475 cm^{-1} are, according to the literature, associated with bending (deformation) vibrations (δ) of the O-Y-O and/or O-Yb-O bonds [55,56]. An analysis of the recorded spectra made it possible to conclude that the absorption bands of the individual phases studied do not differ significantly, which proves that the phases are isostructural with respect to each other. The maxima of the absorption bands with an increase in the concentration of Yb^{3+} ions in the crystal lattice of the obtained $Y_{1-x}Yb_xVO_4$ solid solution only slightly shift towards lower values of the wave numbers. Thus, the results of IR tests are additional confirmation that a continuous substitutional solid solution of $Y_{1-x}Yb_xVO_4$ with a YVO_4 or $YbVO_4$ structure is formed in the YVO_4–$YbVO_4$ system. The structure of this solution is built from interconnected corners and/or edges of VO_4 tetrahedra and Y(Yb)O_6 octahedra.

The next study in this work, to which the synthesized phases YVO_4 (Figure 6a), $YbVO_4$ (Figure 6e), and the solid solution $Y_{1-x}Yb_xVO_4$ for x = 0.10, 0.50, 0.90 (Figure 6b–d) were subjected, was the UV-Vis-DRS. The UV-Vis-DR reflectance spectra recorded for the samples as a function of radiation energy were subjected to the Kubelka–Munk transformation to estimate their energy gap value.

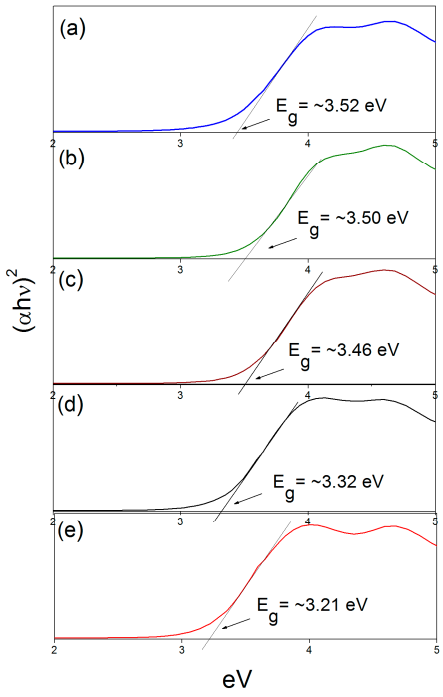

Figure 6. The relationship $(\alpha h\nu)^2$ as a function of the photon energy hν with the determined value of the energy gap Eg for: (**a**) YVO_4, (**b**) $Y_{0.90}Yb_{0.10}VO_4$, (**c**) $Y_{0.50}Yb_{0.50}VO_4$, (**d**) $Y_{0.10}Yb_{0.90}VO_4$, (**e**) $YbVO_4$.

The value of the energy gap for the studied phases was determined from the intersection of the tangent drawn to the rectilinear part of the graph $K^2 = f(E)$ with the abscissa axis, i.e., the energy, as shown in Figure 6.

The determined values of the energy gap (Eg) for YVO_4 and $YbVO_4$ are ~3.52 eV and ~3.21 eV, while the value of the energy gap for the solid solution decreases with increasing x, i.e., from Eg = ~3.50 eV for $Y_{0.90}Yb_{0.10}VO_4$ to ~3.32 eV for $Y_{0.10}Yb_{0.90}VO_4$ [41].

Based on the results obtained, it was concluded that the $Y_{1-x}Yb_xVO_4$ solid solution belongs to the group of wide energy gap semiconductors.

3.2. High-Temperature Treatment

In addition to the mechanochemically synthesized solutions obtained from the YVO_4–$YbVO_4$ system, five samples of the solution (with identical compositions as in the first part of this work, Table 1) were prepared using the classical method of high-temperature solid-state reactions. Adequately, the substrates for the preparation of the mixtures, i.e., YVO_4 and $YbVO_4$, were also obtained by using the high-temperature method [3,5,6]. Mixtures of YVO_4 with $YbVO_4$ (Table 1) after homogenization were heated in the following steps: I—1000 °C (12 h) → II—1200 °C (12 h) → III—1400 °C (12 h) → IV—1500 °C (12 h) (Figure 7).

The heating conditions of the samples were chosen so that the reactions occurring in the mixtures would proceed in a solid state, i.e., the substrates would not undergo both melting and consolidation. It is safe to choose these temperatures so that they do not exceed both the temperature of any eutectic forming between the substrates and the Tamman temperature. Figure 7 presents fragments of diffractograms of an equimolar mixture of YVO_4 + $YbVO_4$ (Figure 7a) before heating compared with fragments of diffractograms of the $Y_{1-x}Yb_xVO_4$ solid solution for x = 0.50 (Figure 7b) after heating at a temperature of 1500 °C (12 h).

The XRD phase analysis showed that all the samples investigated changed their phase composition after the fourth stage of their heating. Based on the XRD phase analysis of samples 1–5 after this stage of their heating, i.e., at 1500 °C for 12 h, they were found to be monophasic and to contain only the $Y_{1-x}Yb_xVO_4$ solid solution (Figures 7b and 8).

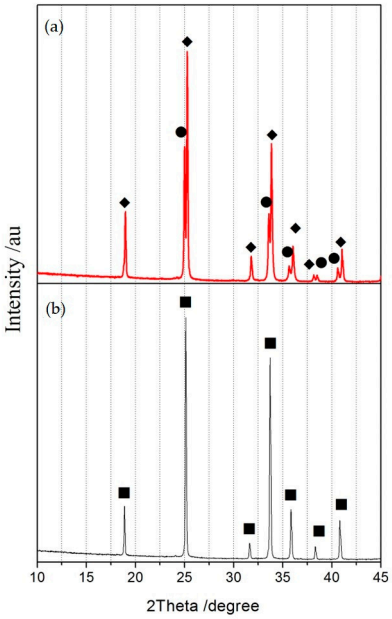

Figure 7. Fragments of diffractograms: (**a**) $YbVO_4$ (◆) + YVO_4 (●), (**b**) $Y_{0.50}Yb_{0.50}VO_4$ (■).

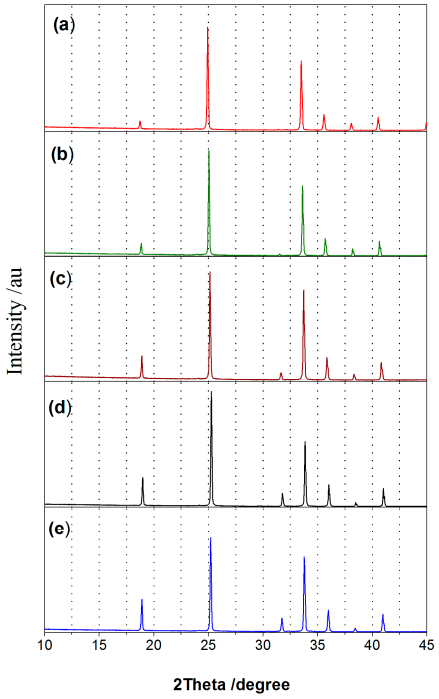

Figure 8. Fragments of diffractograms: (**a**) YVO_4, (**b**) $Y_{0.90}Yb_{0.10}VO_4$, (**c**) $Y_{0.50}Yb_{0.50}VO_4$, (**d**) $Y_{0.10}Yb_{0.90}VO_4$, (**e**) $YbVO_4$.

The fact that only the $Y_{1-x}Yb_xVO_4$ solid solution was present in the samples was evidenced by the lines registered on their diffractograms, which corresponded to interplane distances falling within the range of values characteristic of analogous lines in the XRD set of pure YVO_4 and $YbVO_4$. Both the position of the diffraction lines and their respective intensities were consistent with the results presented in the papers [5,6,35,38,41].

On the basis of the results obtained, it was confirmed that by the method of high-temperature reactions occurring in the solid state in an air atmosphere, a solid solution with the general formula $Y_{1-x}Yb_xVO_4$ was obtained over the entire range of concentrations of the components of the studied system.

Figure 8 presents fragments of the diffractograms of the high-temperature treatment obtained, compounds YVO_4 (Figure 8a) and $YbVO_4$ (Figure 8e), compared with fragments of the diffractograms of the $Y_{1-x}Yb_xVO_4$ solid solution for x = 0.10 (Figure 8b), x = 0.50 (Figure 8c), and x = 0.90 (Figure 8d).

Further experiments were aimed at confirming that the $Y_{1-x}Yb_xVO_4$ solid solution obtained by the high-temperature treatment method crystallizes in a tetragonal system. For this purpose, powder diffractograms of the $Y_{1-x}Yb_xVO_4$ solution for x = 0.10, 0.25, 0.50, 0.75, and 0.90 were subjected to refinement (REFINEMENT program). Based on the results obtained, it was confirmed that the solid solution obtained by this method also crystallizes in a tetragonal system, and the parameters of its elementary cells were determined. Table 4 presents the calculated parameters of the elementary cells of their volumes and X-ray and experimental densities for the synthesized solid solution.

Table 4. Unit cell parameters, volumes and densities of solid solution $Y_{1-x}Yb_xVO_4$ for x = 0.10, 0.25, 0.50, 0.75, and 0.90 obtained by high-temperature treatment.

x in $Y_{1-x}Yb_xVO_4$	a, b [nm]	c [nm]	α, β, γ [°]	V [nm^3]	d_{xrd}/d_{exp} [g/cm^3]
0.10	0.71097	0.62832	90.00	0.3176	4.44/4.40 ± 0.05
0.25	0.70933	0.62739	90.00	0.3157	4.73/4.71 ± 0.05
0.50	0.70803	0.62677	90.00	0.3142	5.20/5.19 ± 0.05
0.75	0.70566	0.62523	90.00	0.3113	5.70/5.67 ± 0.05
0.90	0.70473	0.62475	90.00	0.3103	5.99/5.97 ± 0.05

The obtained results (Table 4) indicate that with an increasing value of x in $Y_{1-x}Yb_xVO_4$, i.e., with an increasing degree of the incorporation of Yb^{3+} ions in place of Y^{3+}—similar to this solid solution obtained by the mechanochemical method—there is a contraction of the crystal lattice, i.e., the volume of elementary cells decreases. An analysis of these data in comparison with analogous ones for the mechanochemical method indicates, moreover, that the volume of elementary cells for the solution obtained by the high-temperature method is always smaller. It is this volume, among other things, that influences the higher values of density, both X-ray and experimental. These presented differences are due to the lower degree of structure defection and porosity of the solution obtained at high temperatures (from 1000–1500 °C).

Scanning electron microscopy (SEM) studies of the compounds YVO_4 and $YbVO_4$, as well as the solid solution $Y_{1-x}Yb_xVO_4$ for x = 0.50 (Figure 9) obtained by the high-temperature treatment method, allowed us to conclude that the crystallites of the solid solution $Y_{0.5}Yb_{0.5}VO_4$ are very similar to those of the matrices, i.e., YVO_4 and $YbVO_4$, in terms of shape.

From the SEM images shown in Figure 9, with 10,000 zoom, it can be seen that the size of the solution crystallites differs from that of the substrates. Although the sizes are more diverse, some are larger, averaging 8μm. Moreover, these crystallites, as expected, are significantly larger than the crystallites of the solid solution obtained mechanochemically.

Using the LDS method, the particle size distribution of the $Y_{1-x}Yb_xVO_4$ solid solution obtained by the high-temperature treatment method was determined (Figure 10).

The particle sizes of the $Y_{1-x}Yb_xVO_4$ solid solution obtained by the high-temperature treatment method, unlike those of the solution obtained by the mechanochemical method, have micrometer sizes, i.e., of ~0.61 μm for x = 0.10, ~0.64 μm for x = 0.25, ~0.31 μm for x = 0.50, ~0.36 μm for x = 0.75, and ~0.33 μm for x = 0.90. In addition, based on the LDS curves, the particle size distribution of the $Y_{1-x}Yb_xVO_4$ solution obtained by the HT method was found to be inhomogeneous (Figure 10).

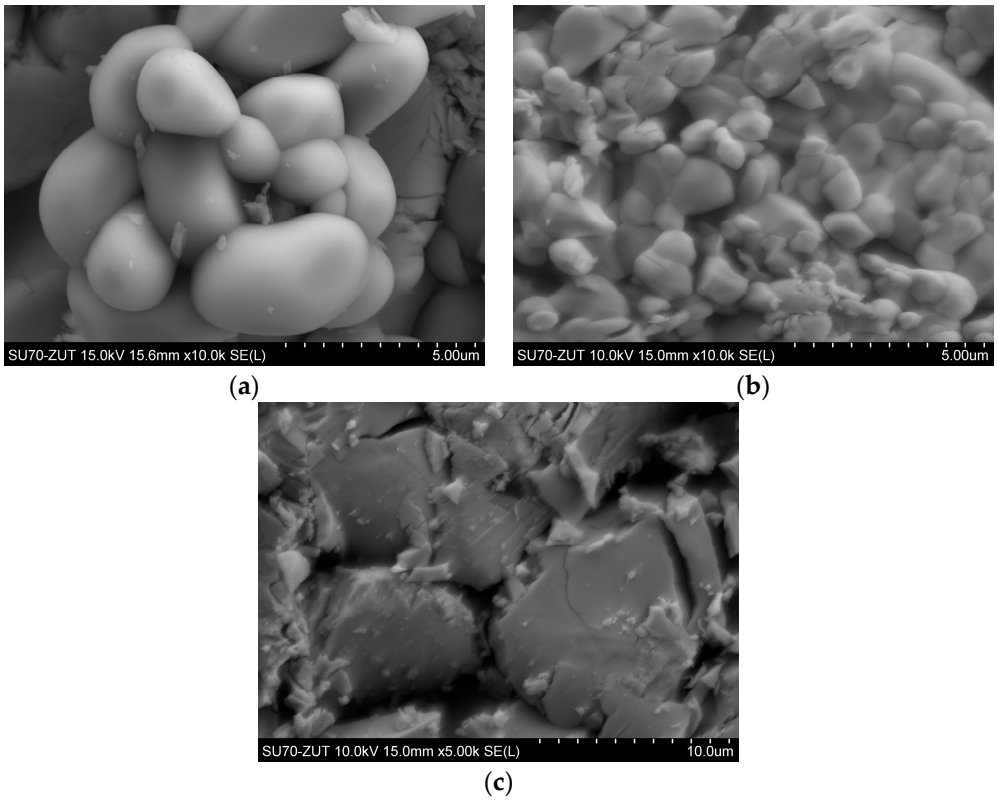

Figure 9. SEM images of (**a**) $YbVO_4$, (**b**) YVO_4, (**c**) $Y_{0.50}Yb_{0.50}VO_4$ obtained by high-temperature treatment.

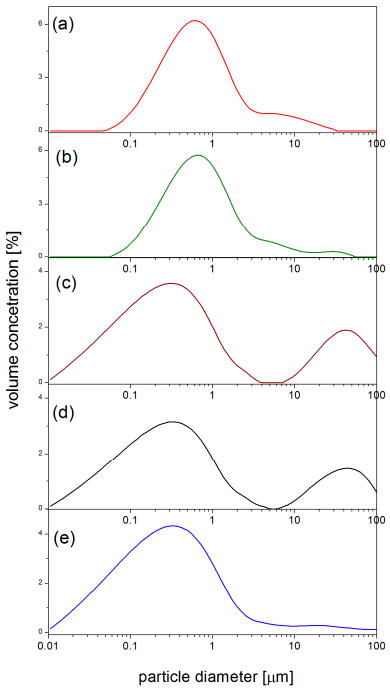

Figure 10. Particle size distribution curve of: (**a**) $Y_{0.90}Yb_{0.10}VO_4$, (**b**) $Y_{0.75}Yb_{0.25}VO_4$, (**c**) $Y_{0.50}Yb_{0.50}VO_4$, (**d**) $Y_{0.25}Yb_{0.75}VO_4$, (**e**) $Y_{0.10}Yb_{0.90}VO_4$ (high-temperature treatment).

In order to initially confirm that the $Y_{1-x}Yb_xVO_4$ solution synthesized by the second method exhibits the YVO_4 structure, IR investigations were carried out. In addition to the IR spectra of the YVO_4 (Figure 11a) and $YbVO_4$ (Figure 11e) compounds, the IR spectra

of the obtained $Y_{1-x}Yb_xVO_4$ solid solution for x = 0.10, 0.50, 0.90 (Figure 11b–d) are also shown in Figure 11.

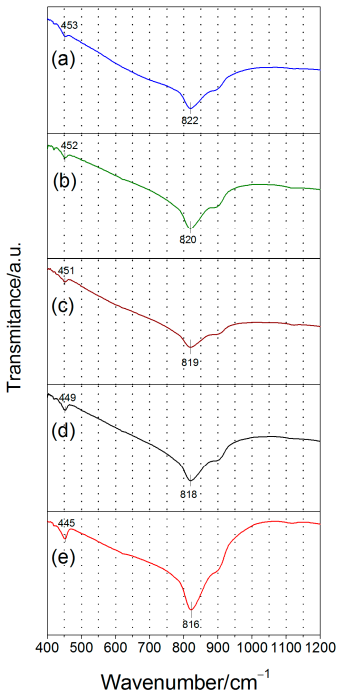

Figure 11. IR spectrum of: (**a**) YVO_4, (**b**) $Y_{0.90}Yb_{0.10}VO_4$, (**c**) $Y_{0.50}Yb_{0.50}VO_4$ (**d**) $Y_{0.10}Yb_{0.90}VO_4$, (**e**) $YbVO_4$.

In the IR spectra of the studied phases obtained by the high-temperature treatment method in the wavelength number range from 400 to 1200 cm^{-1}, two narrow absorption bands were registered (Figure 11), which are located in the same wavelength number ranges as the absorption bands registered on the IR spectra of the phases obtained by the high-energy ball milling method (Figure 5). The difference is that the bands for the HT method are much narrower and more formed. Based on the literature [53–55], these bands can be attributed to both the stretching vibrations of V-O bonds in VO_4 tetrahedra, and the stretching vibrations of Y-O or Yb-O bonds in YO_6 or YbO_6 octahedra. At the same time, it was found that as the degree of the incorporation of Yb^{3+} ions in place of Y^{3+} into the YVO_4 crystal lattice increased, the recorded absorption bands of the solid solution (Figure 11b–d) shifted slightly towards lower wave number values. The results of this part of the work also confirmed that the $Y_{1-x}Yb_xVO_4$ solid solution obtained by the high-temperature treatment method exhibits a YVO_4 structure and is composed of VO_4 tetrahedra and $Y(Yb)O_6$ octahedra.

Phases obtained by high-temperature treatment (HT): YVO_4 (Figure 12a), $YbVO_4$ (Figure 12e) and the solid solution $Y_{1-x}Yb_xVO_4$ for x = 0.10, 0.50, 0.90 (Figure 12b–d) in the last stage of the work were subjected to UV-Vis-DRS to estimate their energy gap values.

The determined values of the energy gap (Eg) for YVO_4 and $YbVO_4$ are, respectively, ~3.66 eV and ~3.55 eV, while the value of the energy gap for the solid solution decreases with increasing x, i.e., from Eg = ~3.62 eV for $Y_{0.90}Yb_{0.10}VO_4$ to ~3.57 eV for $Y_{0.10}Yb_{0.90}VO_4$ [41]. It was additionally determined that the energy gap values for the $Y_{1-x}Yb_xVO_4$ solution obtained by high-temperature treatment are slightly higher than the gap values for this solution obtained by high-energy ball milling. These differences are undoubtedly influenced by the size of the crystallites (the larger the crystallites, the higher the Eg value). Based on the results, it was concluded that the $Y_{1-x}Yb_xVO_4$ solid solution obtained by both methods belongs to the group of semiconductors with a wide energy gap.

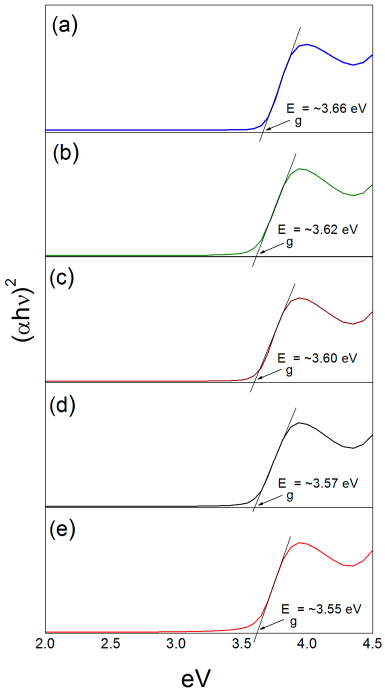

Figure 12. The relationship $(\alpha h\nu)^2$ as a function of the photon energy hν with the determined value of the energy gap Eg for: (**a**) YVO_4, (**b**) $Y_{0.90}Yb_{0.10}VO_4$, (**c**) $Y_{0.50}Yb_{0.50}VO_4$, (**d**) $Y_{0.10}Yb_{0.90}VO_4$, (**e**) $YbVO_4$.

The obtained solid solution may find potential application not only as a photocatalyst, but also, for example, as a component of optoelectronic materials.

4. Conclusions

The results of the conducted research allowed us to achieve the main goal of the work, i.e., to experimentally confirm that a continuous substitution solid solution of the general formula $Y_{1-x}Yb_xVO_4$, where $0.00 < x < 1.00$, is formed in the YVO_4–$YbVO_4$ system.

The solution was obtained from mixtures YVO_4 with $YbVO_4$ by the high-temperature method, as well as by the high-energy ball milling method, which was used for the first time for the presented purpose.

The solid solution obtained mechanochemically is nanocrystalline, while the high-temperature treatment one is microcrystalline. With the increase of x in $Y_{1-x}Yb_xVO_4$ obtained by both methods, the crystal lattice of the solid solution contracted. Based on the LDS curves, the particle size distribution of the $Y_{1-x}Yb_xVO_4$ solution obtained by the two methods was found to be inhomogeneous. The structure of the solid solution obtained by both alternative synthesis methods consists of connected VO_4 tetrahedra with $Y(Yb)O_6$ octahedra. The energy gap values for the $Y_{1-x}Yb_xVO_4$ solution obtained by the high-temperature treatment method are slightly higher than the gap values for this solution obtained by the high-energy ball milling method. Regardless of the method of synthesis, $Y_{1-x}Yb_xVO_4$ solid solutions belong to the group of wide energy gap semiconductors.

Differences in the physicochemical properties of the solution depending on the method of its synthesis are primarily due to differences in the size of their crystallites.

Author Contributions: Conceptualization, M.P. and E.F.; methodology, M.P. and E.F.; validation, M.P., E.F. and D.K.; formal analysis, M.P. and E.F.; investigation, M.P., E.F., D.K. and P.K.; data curation, M.P. and D.K.; writing—original draft preparation, M.P.; writing—review and editing, E.F.; visualization, M.P.; supervision, E.F. All authors have read and agreed to the published version of the manuscript.

Funding: This research received no external funding.

Institutional Review Board Statement: Not applicable.

Informed Consent Statement: Not applicable.

Data Availability Statement: The data presented in this study are available on request from the corresponding author.

Conflicts of Interest: The authors declare no conflict of interest.

References

1. Baláž, P.; Achimovicová, M.; Baláž, M.; Billik, P.; Zara, C.Z.; Criado, J.M.; Delogu, F.; Dutková, E.; Gaffet, E.; Gotor, F.J.; et al. Hallmarks of Mechanochemistry: From Nanoparticles to Technology. *Chem. Soc. Rev.* **2013**, *42*, 7571–7637. [CrossRef]
2. Kutuk, S. Influence of Milling Parameters on Particle Size of Ulexite Material. *Powder Technol.* **2016**, *301*, 421–428. [CrossRef]
3. Piz, M.; Dulian, P.; Filipek, E.; Wieczorek-Ciurowa, K.; Kochmanski, P. Characterization of Phases in the V_2O_5–Yb_2O_3 System Obtained by High-Energy Ball Milling and High-Temperature Treatment. *J. Mater. Sci.* **2018**, *53*, 13491–13500. [CrossRef]
4. Dulian, P.; Bąk, W.; Piz, M.; Garbarz-Glos, B.; Sachuk, O.V.; Wieczorek-Ciurowa, K.; Lisińska-Czekaj, A.; Czekaj, D. Mg^{2+} Doping Effects on the Structural and Dielectric Properties of $CaCu_3Ti_4O_{12}$ Ceramics Obtained by Mechanochemical Synthesis. *Materials* **2021**, *14*, 1187. [CrossRef]
5. Levin, E.M. The System Y_2O_3-V_2O_5. *J. Am. Ceram. Soc.* **1978**, *50*, 381–382. [CrossRef]
6. Brusset, H.; Madaule-Aubry, F.; Blanck, B.; Glaziou, J.P.; Laude, J.P. Etude Des Oxydes Mixtes de Lanthanides et de Vanadium(V). *Can. J. Chem.* **1971**, *49*, 3700–3707. [CrossRef]
7. Yu, Y.; Cheng, Y.; Zhang, H.; Wang, J.; Cheng, X.; Xia, H. Growth and Thermal Properties of $YbVO_4$ Single Crystal. *Mater. Lett.* **2006**, *60*, 1014–1018. [CrossRef]
8. Eghbali-Arani, M.; Sobhani-Nasab, A.; Rahimi-Nasrabadi, M.; Ahmadi, F.; Pourmasoud, S. Ultrasound-Assisted Synthesis of $YbVO_4$ Nanostructure and $YbVO_4$/$CuWO_4$ Nanocomposites for Enhanced Photocatalytic Degradation of Organic Dyes under Visible Light. *Ultrason. Sonochem.* **2018**, *43*, 120–135. [CrossRef]
9. Gao, Y.; Fan, M.; Fang, Q.; Han, W. Controllable Synthesis, Morphology Evolution and Luminescence Properties of $YbVO_4$ Microcrystals. *New J. Chem.* **2013**, *37*, 670–678. [CrossRef]
10. Fuess, H.; Kallel, A.; Neutronique, D.; Cedex, C.E.N.G.; Temp, K. Refinement of the Crystal Structure of Some Rare Earth Vanadates RVO_4 (R = Dy, Tb, Ho, Yb). *J. Solid State Chem.* **1972**, *14*, 11–14. [CrossRef]
11. Baglio, J.A.; Sovers, O.J. Crystal Structures of the Rare-Earth Orthovanadates. *J. Solid State Chem.* **1971**, *3*, 458–465. [CrossRef]
12. Cheng, Y.; Zhang, H.; Zhang, K.; Xin, Z.; Yang, X.; Xu, X.; Gao, W.; Li, D.; Zhao, C.; Xu, J. Growth and Spectroscopic Characteristics of Er^{3+}:$YbVO_4$ Crystal. *J. Cryst. Growth* **2009**, *311*, 3963–3968. [CrossRef]
13. Liu, F.Q.; Sun, S.Q.; Gao, C.Y.; Xu, J.Q. Optical Properties of Nd:$YbVO_4$ Crystal. *Opt. Appl.* **2015**, *45*, 63–70. [CrossRef]
14. Miura, B.A.; Ferreira, N.H.; Oliveira, P.F.; De Faria, E.H.; Tavares, D.C.; Rocha, L.A.; Ciuffi, K.J.; Nassar, E.J. Functionalization of Luminescent YVO_4:Eu^{3+} Nanoparticles by Sol-Gel. *J. Lumin.* **2015**, *159*, 93–99. [CrossRef]
15. He, F.; Yang, P.; Niu, N.; Wang, W.; Gai, S.; Wang, D.; Lin, J. Hydrothermal Synthesis and Luminescent Properties of YVO_4:Ln^{3+} (Ln = Eu, Dy, and Sm) Microspheres. *J. Colloid Interface Sci.* **2010**, *343*, 71–78. [CrossRef]
16. Li, G.; Chao, K.; Peng, H.; Chen, K. Hydrothermal Synthesis and Characterization of YVO_4 and YVO_4:Eu^{3+} Nanobelts and Polyhedral Micron Crystals. *J. Phys. Chem. C* **2008**, *112*, 6228–6231. [CrossRef]
17. Erdei, S.; Ainger, F.W.; Cross, L.E.; White, W.B. Hydrolyzed Colloid Reaction (HCR) Technique for Preparation of YVO_4, YPO_4, $YV_xP_{1-x}O_4$. *Mater. Lett.* **1994**, *21*, 143–147. [CrossRef]
18. LeBret, J.B.; Norton, M.G.; Bahr, D.F. Examination of Crystal Defects with High-KV X-Ray Computed Tomography. *Mater. Lett.* **2005**, *59*, 1113–1116. [CrossRef]
19. Lebret, J.B.; Norton, M.G.; Bahr, D.F.; Field, D.P.; Lynn, K.G. Characterization of Low Angle Grain Boundaries in Yttrium Orthovanadate. *J. Mater. Sci.* **2005**, *40*, 3347–3353. [CrossRef]
20. Yu, M.; Lin, J.; Wang, Z.; Fu, J.; Wang, S.; Zhang, H.J.; Han, Y.C. Fabrication, Patterning, and Optical Properties of Nanocrystalline YVO_4:A (A = Eu^{3+}, Dy^{3+}, Sm^{3+}, Er^{3+}) Phosphor Films via Sol-Gel Soft Lithography. *Chem. Mater.* **2002**, *14*, 2224–2231. [CrossRef]
21. Cheng, Z.; Xing, R.; Hou, Z.; Huang, S.; Lin, J. Patterning of Light-Emitting YVO_4:Eu^{3+} Thin Films via Inkjet Printing. *J. Phys. Chem. C* **2010**, *114*, 9883–9888. [CrossRef]
22. Chen, J.; Guo, F.; Zhuang, N.; Lan, J.; Hu, X.; Gao, S. A Study on the Growth of Yb:YVO_4 Single Crystal. *J. Cryst. Growth* **2002**, *243*, 450–455. [CrossRef]
23. Zhong, D.; Teng, B.; Li, J.; Zhang, S.; Zhang, B.; Wang, C.; Tian, X.; Liu, J. Growth and Laser Action of Yb: YVO_4 Crystals with Low Yb Doping Concentration. *J. Cryst. Growth* **2012**, *358*, 16–19. [CrossRef]
24. Voron'ko, Y.K.; Kochurikhin, V.V.; Sobol', A.A.; Ushakov, S.N.; Shukshin, V.E. Growth and Spectroscopic Study of Yb^{3+}-Activated YVO_4 Crystals. *Inorg. Mater.* **2004**, *40*, 1083–1087. [CrossRef]
25. Klassen, A.V.; Matsukura, M.; Nakamura, O.; Kochurikhin, V.V.; Ivanov, M.A.; Orlova, G.Y.; Miyamoto, A.; Furukawa, Y. Edge-Defined Film-Fed Growth of Yb:YVO_4 Single Crystal Plates. *J. Cryst. Growth* **2008**, *310*, 2895–2898. [CrossRef]
26. Zhang, Q.; Saito, F. A Review on Mechanochemical Syntheses of Functional Materials. *Adv. Powder Technol.* **2012**, *23*, 523–531. [CrossRef]
27. Au, C.T.; Zhang, W.D.; Wan, H.L. Preparation and Characterization of Rare Earth Orthovanadates for Propane Oxidative Dehydrogenation. *Catal. Lett.* **1996**, *37*, 241–246. [CrossRef]

28. Tojo, T.; Zhang, Q.; Saito, F. Mechanochemical Synthesis of Rare Earth Orthovanadates from R_2O_3 (R = Rare Earth Elements) and V_2O_5 Powders. *J. Alloys Compd.* **2007**, *427*, 219–222. [CrossRef]
29. Erdei, S. Preparation of YVO_4 Powder from the Y_2O_3 + V_2O_5 + H_2O System by a Hydrolysed Colloid Reaction (HCR) Technique. *J. Mater. Sci.* **1995**, *30*, 4950–4959. [CrossRef]
30. Wang, X.; Loa, I.; Syassen, K.; Hanfland, M.; Ferrand, B. Structural Properties of the Zircon- and Scheelite-Type Phases of YVO_4 at High Pressure. *Phys. Rev. B Condens. Matter* **2004**, *70*, 3–8. [CrossRef]
31. Souad, M.; Mohammed, S.; Mohamed, D.; Claude, D. The Effect of Pressure on the Structural and Electronic Properties of Yttrium Orthovanadate YVO_4 Compound: Total-Energy Calculations. *Z. FürKrist. Cryst. Mater.* **2010**, *225*, 514–519. [CrossRef]
32. Chakoumakos, B.C.; Abraham, M.M.; Boatner, L.A. Crystal Structure Refinements of Zircon-Type MVO_4 (M = Sc, Y, Ce, Pr, Nd, Tb, Ho, Er, Tm, Yb, Lu). *J. Solid State Chem.* **1994**, *109*, 197–202. [CrossRef]
33. Wiglusz, R.J.; Marciniak, L.; Pazik, R.; Strek, W. Structural and Spectroscopic Characterization of Nd^{3+}-Doped YVO_4 Yttrium Orthovanadate Nanocrystallites. *Cryst. Growth Des.* **2014**, *14*, 5512–5520. [CrossRef]
34. Reitz, C.; Smarsly, B.; Brezesinski, T. General Synthesis of Ordered Mesoporous Rare-Earth Orthovanadate Thin Films and Their Use as Photocatalysts and Phosphors for Lighting Applications. *ACS Appl. Nano Mater.* **2019**, *2*, 1063–1071. [CrossRef]
35. Errandonea, D.; Garg, A.B. Recent Progress on the Characterization of the High-Pressure Behaviour of AVO_4 Orthovanadates. *Prog. Mater. Sci.* **2018**, *97*, 123–169. [CrossRef]
36. Kolesnikov, I.E.; Golyeva, E.V.; Kurochkin, M.A.; Kolesnikov, E.Y.; Lähderanta, E. Concentration Series of Sm^{3+}-Doped YVO_4 Nanoparticles: Structural, Luminescence and Thermal Properties. *J. Lumin.* **2020**, *219*, 116946. [CrossRef]
37. Getz, M.N.; Nilsen, O.; Hansen, P.A. Sensors for Optical Thermometry Based on Luminescence from Layered YVO_4: Ln^{3+} (Ln = Nd, Sm, Eu, Dy, Ho, Er, Tm, Yb) Thin Films Made by Atomic Layer Deposition. *Sci. Rep.* **2019**, *9*, 1–11. [CrossRef]
38. Dai, Y.; Chen, J.; Tang, Y.; Xiang, H.; Li, J.; Fang, L. Relationship between Bond Characteristics and Microwave Dielectric Properties of $REVO_4$ (RE = Yb, Ho) Ceramics. *Ceram. Int.* **2023**, *49*, 875–881. [CrossRef]
39. Wang, S.; Wang, P.; Ruan, Y.; Wang, Y.; Zhang, S. Photoluminescence Characteristics and Energy Transfer Phenomena in Ce^{3+}-Doped YVO_4 single Crystal. *Sci. Eng. Compos. Mater.* **2021**, *28*, 205–214. [CrossRef]
40. Zhao, B.; Ye, Y.; Chen, J.; Lin, H.; Zhang, G.; Mateos, X.; Serres, J.M.; Aguiló, M.; Díaz, F.; Loiko, P.; et al. Growth, Spectroscopy, and Laser Operation of "Mixed" Vanadate Crystals Yb:Lu_{1-x}-YY_xLayVO_4. *Opt. Mater. Express* **2018**, *8*, 493. [CrossRef]
41. Vadivel, S.; Paul, B.; Kumaravel, M.; Hariganesh, S.; Rajendran, S.; Prasanga Gayanath Mantilaka, M.M.M.G.; Mamba, G.; Puviarasu, P. Facile Synthesis of $YbVO_4$, and YVO_4 Nanostructures through MOF Route for Photocatalytic Applications. *Inorg. Chem. Commun.* **2020**, *115*, 107855. [CrossRef]
42. Ćirić, A.; Stojadinović, S.; Dramićanin, M.D. Time-Integrated Luminescence Thermometry of Eu^{3+} and Dy^{3+} Doped YVO_4. *Sens. Actuators A Phys.* **2019**, *295*, 450–455. [CrossRef]
43. Wang, Y.; Song, X.X.; Tang, W.J.; Jia, C.L. Multi-Wavelength Emission from Er-Implanted $YbVO_4$ Crystal. *Phys. Solid State* **2020**, *62*, 1067–1073. [CrossRef]
44. Kolesnikov, I.E.; Mamonova, D.V.; Kurochkin, M.A.; Kolesnikov, E.Y.; Lähderanta, E. Optical Thermometry by Monitoring Dual Emissions from YVO_4 and Eu^{3+} in YVO_4:Eu^{3+} Nanoparticles. *ACS Appl. Nano Mater.* **2021**, *4*, 1959–1966. [CrossRef]
45. Pourmasoud, S.; Sobhani-Nasab, A.; Behpour, M.; Rahimi-Nasrabadi, M.; Ahmadi, F. Investigation of Optical Properties and the Photocatalytic Activity of Synthesized $YbYO_4$ Nanoparticles and $YbVO_4$/$NiWO_4$ Nanocomposites by Polymeric Capping Agents. *J. Mol. Struct.* **2018**, *1157*, 607–615. [CrossRef]
46. Rivera-Enríquez, C.E.; Fernández-Osorio, A.L. Synthesis of YVO_4:Eu^{3+} Nanophosphors by the Chemical Coprecipitation Method at Room Temperature. *J. Lumin.* **2021**, *236*, 118110. [CrossRef]
47. Blonska-Tabero, A.; Bosacka, M.; Filipek, E.; Piz, M.; Kochmanski, P. High-Temperature Synthesis and Unknown Properties of $M_3Cr_4(PO_4)_6$, Where M = Zn or Mg and a New Solid Solution $Zn_{1.5}Mg_{1.5}Cr_4(PO_4)_6$. *J. Therm. Anal. Calorim.* **2020**, *140*, 2625–2631. [CrossRef]
48. Filipek, E.; Paczesna, A.; Piz, M. $Sr_2InV_3O_{11}$—New Ceramic Compound in $Sr_2V_2O_7$–$InVO_4$ System and Its Characteristic. *Ceram. Int.* **2016**, *42*, 14148–14154. [CrossRef]
49. Piz, M.; Filipek, E. Synthesis and Homogeneity Range of $Yb_{8-x}Y_xV_2O_{17}$ in the $Yb_8V_2O_{17}$–$Y_8V_2O_{17}$ System. *J. Therm. Anal. Calorim.* **2017**, *130*, 277–283. [CrossRef]
50. Dąbrowska, G.; Filipek, E.; Tabero, P. New Solid Solution and Phase Equilibria in the Subsolidus Area of the Three-Component CuO–V_2O_5–Ta_2O_5 Oxide System. *Materials* **2022**, *15*, 232. [CrossRef]
51. Kutuk-Sert, T. Stability Analyses of Submicron-Boron Mineral Prepared by Mechanical Milling Process in Concrete Roads. *Constr. Build. Mater.* **2016**, *121*, 255–264. [CrossRef]
52. Kutuk-Sert, T.; Ozturk, M.; Kutuk, S. Digital Image Processing of Warm Mix Asphalt Enriched with Nanocolemanite and Nanoulexite Minerals. *Constr. Build. Mater.* **2023**, *399*, 132542. [CrossRef]
53. Vucinic-Vasic, M.; Kremenovic, A.; Nikolic, A.S.; Colomban, P.; Mazzerolles, L.; Kahlenberg, V.; Antic, B. Core and Shell Structure of Ytterbium Sesquioxide Nanoparticles. *J. Alloys Compd.* **2010**, *502*, 107–111. [CrossRef]
54. Garg, A.B.; Rao, R.; Sakuntala, T.; Wani, B.N.; Vijayakumar, V. Phase Stability of $YbVO_4$ under Pressure: In Situ x-Ray and Raman Spectroscopic Investigations. *J. Appl. Phys.* **2009**, *106*, 063513. [CrossRef]

55. Vasundhara, K.; Achary, S.N.; Patwe, S.J.; Sahu, A.K.; Manoj, N.; Tyagi, A.K. Structural and Oxide Ion Conductivity Studies on $Yb_{1-x}Bi_xO_{1.5}$ ($0.00 \leq x \leq 0.50$) Composites. *J. Alloys Compd.* **2014**, *596*, 151–157. [CrossRef]
56. Heiba, Z.K.; Akin, Y.; Sigmund, W.; Hascicek, Y.S. X-ray Structure and Microstructure Determination of the Mixed Sesquioxides $(Eu_{1-x}Yb_x)_2O_3$ Prepared by a Sol-Gel Process. *J. Appl. Crystallogr.* **2003**, *36*, 1411–1416. [CrossRef]